Citation
Yuan, C. and Chen, W. and Pham, T.M. and Hao, H. and Chen, L. and Zhang, M. 2020. New epoxy anchor for better bonding between FRP sheets and concrete. Construction and Building Materials. 248: ARTN 118628.
http://doi.org/10.1016/j.conbuildmat.2020.118628

New Epoxy Anchor for Better Bonding between FRP Sheets and Concrete

Cheng Yuan[1], Wensu Chen*[1], Thong M. Pham[1], Hong Hao*[1], Li Chen[2], Mi Zhang[1]

[1] Centre for Infrastructural Monitoring and Protection, School of Civil and Mechanical Engineering, Curtin University, Perth, Australia
[2] School of Civil Engineering, Southeast University, Nanjing, China
**Corresponding Authors*

Abstract

Epoxy anchor was proposed in this study to enhance the interfacial bond strength between basalt fibre reinforced polymer (BFRP) sheets and concrete. Epoxy anchors were formed by drilling holes into the concrete substrate before applying epoxy resin. The depth and diameter of epoxy anchors were designed to enhance the cohesive strength of the interface. The proposed epoxy anchors remarkably enhanced the shear resistance while the progressive FRP debonding was significantly postponed. The experimental results showed 77.49% increment in the bond strength, 86.71% increment in the utilization of BFRP sheets, and 78.10% increase in the peak shear stress on average. A bond strength model by incorporating the effects of strain energy and bonding area of epoxy resin was proposed to analyse the effect of anchorage. The predicted debonding load showed good agreement with the testing data.

Keywords: Fibre reinforced polymer (FRP), Concrete, Interfacial bond, Anchorage

1. Introduction

Externally bonded (EB) fibre-reinforced polymer (FRP) sheets to reinforced concrete (RC) structures is an effective strengthening method [1-5]. However, debonding of FRP has a detrimental effect on the interfacial bond because only 40% of the ultimate strain of the strengthening material can be utilized, which underutilizes the tensile capacity of FRP laminates [6-9]. Previous studies [10, 11] have reported different types of FRP debonding failure, such as concrete cover separation (CC), intermediate crack debonding (IC), and plate end debonding (PE). Such a premature failure mode of FRP debonding significantly lowers the efficiency of the strengthening system [12, 13].

To maximize the utilization of FRP sheets and postpone the debonding process, different anchorage systems have been developed, such as FRP anchors [14-17], FRP U-jacket anchors [1, 18], and mechanical anchors (i.e., anchor bolts) [19-21]. Smith et al. [11] experimentally tested the FRP-strengthened RC slabs with FRP spike anchors and found that the increments of 30% in the load-carrying capacity and 110% in the flexural capacity were achieved by using FRP spike anchors as compared to the control slab. Zhang et al. [14, 16] experimentally investigated the effect of FRP anchor position and number of anchors on the interfacial bond performance and found that the bond performance was significantly affected by anchor position and anchor numbers. Wu and Huang [19] experimentally investigated the effect of steel bolts anchorage system on the interfacial bond capacities. The testing results showed the bond strength of the strengthened concrete beam with anchorage was approximately 8 times the bond strength of the specimen without anchorage.

It was also found that the anchorage location was critical to the interfacial bond performance [14]. Wrapping transverse U-jacket anchors along the entire bonding area was found to be effective in enhancing the shear resistance and delaying premature debonding [1]. Anchoring FRP sheets at their end with anchor bolts can effectively prevent brittle debonding failure and enhance the bond shear resistance and the ductility of the strengthened structures [22-24]. Antoniades et al. [25] experimentally tested the reinforced concrete (RC) walls with hybrid anchorage including steel bolt end anchors, U-jackets and FRP anchors. It was found that the hybrid anchorage system effectively enhanced the bond strength at the end of RC walls. Such anchorage systems can significantly enhance the interfacial bond between FRP and concrete.

However, the preparation and installation of these anchors significantly increase the complication of implementation and the requirement of workmanship.

Various indirect anchorage methods have been also developed to enhance the interfacial shear resistance [26-30]. Near-surface mounted (NSM) method was an indirect way to anchor the FRP composites by increasing the adhesive area between FRP and concrete [31-33]. The concrete grooving method (GM), as a simplified version of NSM, has been recommended by ACI [34] due to its significant enhancement on concrete surface roughness. By grooving the concrete substrates before applying epoxy resin, the interfacial bond strength can be remarkably enhanced with the adhesive area between FRP and concrete [35, 36]. However, the preparation of concrete surface grooves would greatly increase construction works [6].

To simplify the construction process and effectively enhance the interfacial bond behaviour, this study proposes an epoxy anchor system to enhance the interfacial bond between BFRP and concrete that can be easily applied in engineering practice. The development of epoxy anchors in this study was inspired by the mechanisms of FRP spike anchor [37] and epoxy interlocking [6]. The interfacial bonding between FRP and concrete and the interlocking action of the epoxy anchors could enhance the shear resistance and consequently result in higher interfacial bond strength and shear stress. The effect of the proposed epoxy anchors on the interfacial bond performance was investigated by conducting single-lap shear tests. The experimental results including the bond strength, ultimate strain utilization, and bond-slip response are presented and discussed in this paper.

2. Epoxy anchor

Figure 1 (a) illustrates the sketch of the proposed epoxy anchors. Epoxy anchors are cured as hardened epoxy resin in the concrete pre-drilled holes. The interfacial bond strength can be enhanced by the epoxy bonding and interlocking action between epoxy and concrete. The preparation of the epoxy anchors included drilling the designed holes on the concrete block by using a hammer drill as shown in Figure 1 (b), then filling the holes with epoxy resin as shown in Figure 1 (c), and finally bonding BFRP sheets. Prior to preparing epoxy anchor, the concrete substrates were roughened by a needle scaler to remove the weak layer of mortar. The epoxy anchors used in this study had various diameters (d_i) of 6 mm, 10 mm, and 15 mm. The embedment depth (d_e) of anchor was kept unchanged and set as 20 mm, which was less than the thickness of concrete cover. The distance between anchors (L_e) was set as 40 mm, which was less than the effective bond length (i.e. 50 mm in this study). The FRP composite was formed by three layers of BFRP sheets to avoid FRP rupture upon loading. This epoxy anchorage system was proposed to (1) enhance the cracking-resistance of concrete substrate; (2) eliminate or delay the interfacial cracking; and (3) increase the effective interfacial shear stress transfer length.

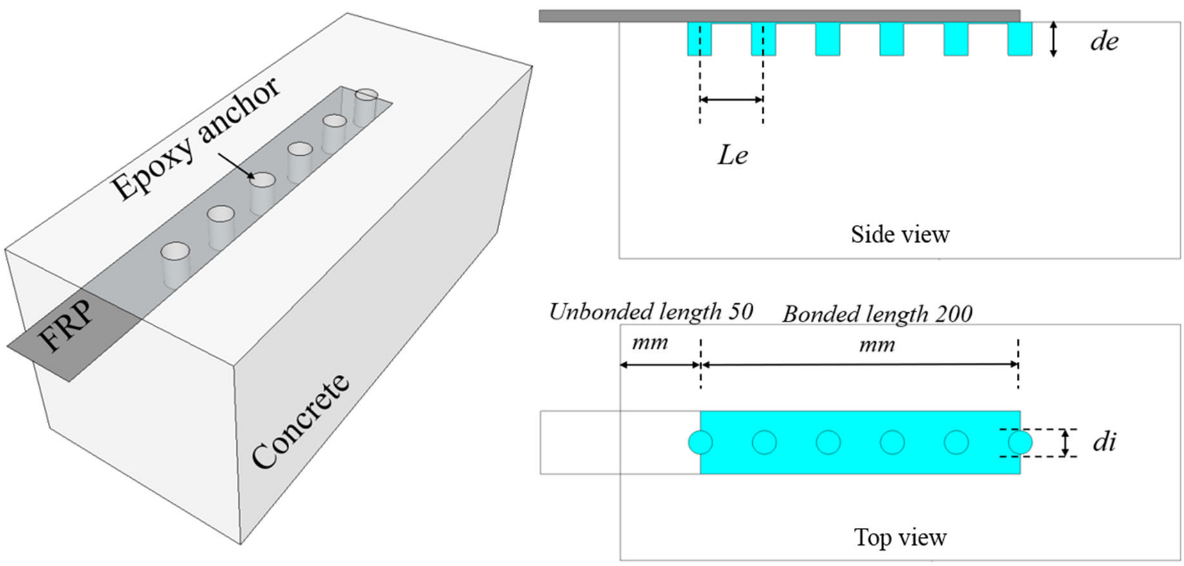

(a) Epoxy anchor: (L) 3D view; (R) 2D view

(b) Hammer drill

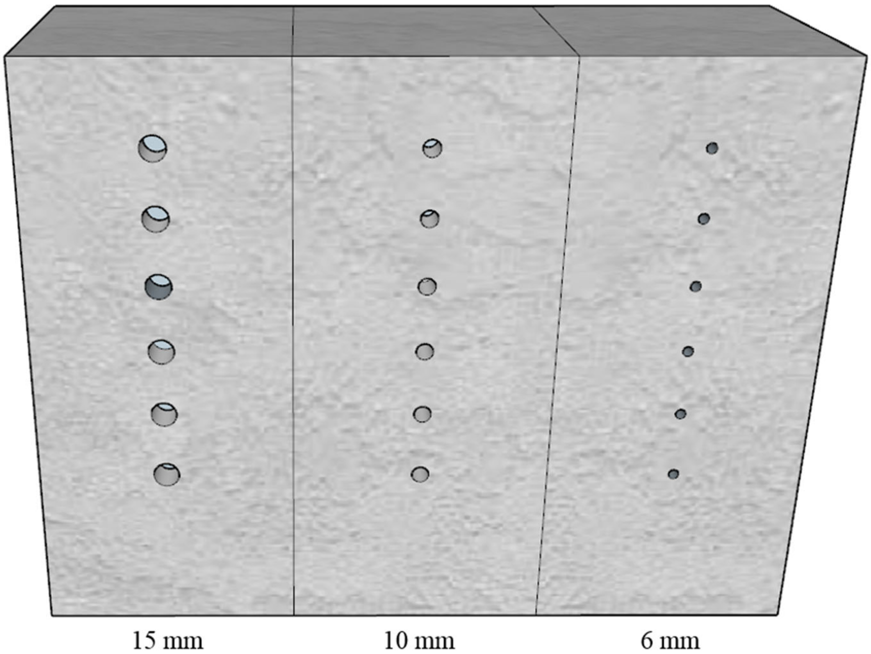

(c) Preparation of concrete surface and holes

Figure 1. Epoxy anchor

3. Material properties

A total of 21 single-lap shear specimens were prepared in this study. Concrete blocks with 150 x 150 x 350 mm^3 in dimensions were prepared as substrates. The maximum coarse aggregate size was 20 mm in the concrete mix. The compressive strength and split tensile strength of the concrete substrates were 40 MPa and 3.90 MPa, respectively. The rupture strain, the ultimate tensile strength, the elastic modulus of basalt fibre-reinforced polymer (BFRP) sheets with the nominal thickness of 0.12 mm was 1.90%, 1333 MPa, and 73 GPa, respectively. The rupture tensile strength, rupture strain and elastic modulus of the epoxy resin was 50.5 MPa, 2.8 GPa and 4.5%, respectively [38]. The specimen details and testing schemes are summarized in Table 1. Figure 2 plots the sketch of the tested specimens, which consider various sizes and numbers of epoxy anchors. The specimen with epoxy anchors was labelled as "*DX-Y-n*". The letter, *DX*, represents the diameter of the anchor (i.e. 6 mm, 10 mm, and 15 mm). The letter, *Y*, represents the number of epoxy anchors (i.e. 1, 2, 3, and 6). The letter, *n*, refers to the number of identical specimens (i.e. 1, 2, and 3).

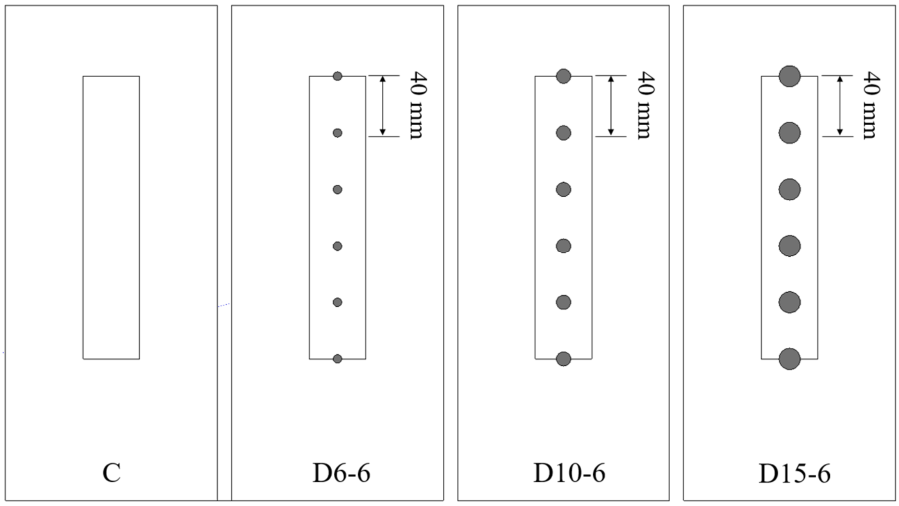

(a) The effect of epoxy anchor size

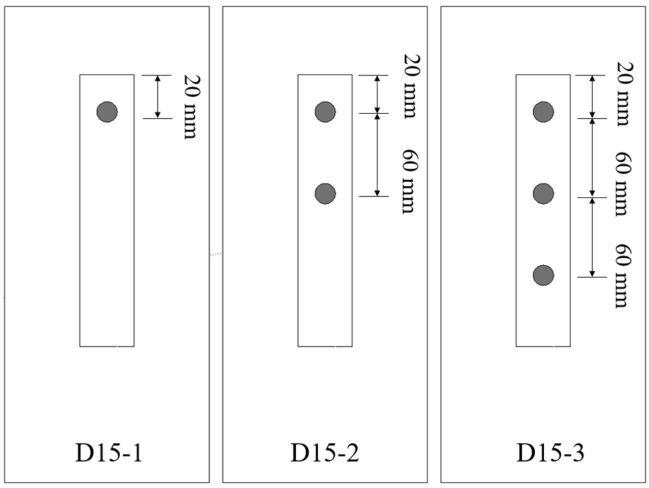

(b) The effect of epoxy anchor number

Figure 2. Schematic diagram of epoxy anchor layout

Table 1. Specimen details and test results

Specimen ID	d_i (mm)	d_e (mm)	L_d (mm)	P_1 (kN)	P_2 (kN)	P_u (kN)	ε_u (%)	τ_m (MPa)	s_o (mm)	G_f (N/mm)	EC (J)	α (mm)	β (mm)	Failure mode
C-1	/	/	/	11.16	11.16	10.84	0.957	4.21	1.62	1.48	7.24	0.20	17.57	C
C-2	/	/	/	9.08	9.08	10.13	0.981	4.19	1.58	1.31	5.87	0.29	21.31	C
C-3	/	/	/	9.11	9.11	11.02	1.012	4.79	1.35	1.64	7.04	0.28	19.59	C
D6-6-1	6	20	40	9.78	10.62	11.86	1.307	4.50	1.79	1.83	7.82	0.15	14.72	C
D6-6-2	6	20	40	9.02	11.56	11.82	1.287	5.74	1.93	1.78	8.70	0.35	20.00	C
D6-6-3	6	20	40	9.71	13.20	14.46	1.298	4.63	1.97	1.47	7.25	0.17	15.49	C
D10-6-1	10	20	40	10.01	13.50	15.63	1.500	5.60	2.22	2.89	10.06	0.19	14.87	C/CE
D10-6-2	10	20	40	9.92	12.29	13.57	1.675	4.35	2.29	2.32	11.32	0.22	18.21	C/CE
D10-6-3	10	20	40	10.53	13.37	13.63	1.569	6.19	2.35	2.51	12.62	0.34	19.00	C/CE
D15-6-1	15	20	40	10.56	18.50	18.61	1.865	8.21	2.34	4.50	17.63	0.24	13.84	C/CE
D15-6-2	15	20	40	12.80	18.25	19.44	1.843	7.47	2.50	4.76	16.97	0.23	14.21	C/CE
D15-6-3	15	20	40	10.76	17.06	18.73	1.800	7.81	2.48	4.19	14.42	0.25	14.47	C/CE
D15-1-1	15	20	40	8.72	15.24	11.89	1.450	5.34	2.25	/	13.28	/	/	C/CE
D15-1-2	15	20	40	11.37	16.58	11.62	1.571	4.89	2.24	/	13.31	/	/	C/CE
D15-1-3	15	20	40	10.20	15.37	11.17	1.462	5.21	1.89	/	11.75	/	/	C/CE
D15-2-1	15	20	40	10.42	15.08	12.32	1.534	5.19	2.49	/	15.03	/	/	C/CE
D15-2-2	15	20	40	8.74	16.15	10.84	1.549	5.46	2.32	/	15.30	/	/	C/CE
D15-2-3	15	20	40	8.81	15.12	12.11	1.671	5.17	2.27	/	15.11	/	/	C/CE
D15-3-1	15	20	40	8.05	15.20	17.30	1.578	6.11	2.71	/	17.45	/	/	C/CE
D15-3-2	15	20	40	8.89	15.42	14.31	1.645	5.52	2.34	/	14.94	/	/	C/CE
D15-3-3	15	20	40	10.31	15.24	11.90	1.649	6.21	2.26	/	14.75	/	/	C/CE

Note: d_i refers to the diameter of epoxy anchor; d_e represents the embedment depth of epoxy anchor; L_d refers to the spacing of epoxy anchors; P_1 is the load of elastic stage; P_2 represents the load of interfacial hardening stage; P_u is the ultimate debonding load; ε_u is the ultimate debonding strain of BFRP sheet; τ_m is the peak shear stress; s_o refers to the peak slip; G_f is the interfacial fracture energy; EC refers to the energy consumption of the debonding process; α and β refer to the fitting coefficients, and "/" means data not available.

4. Experimental program

The single-lap shear tests were carried out to investigate the effect of the proposed epoxy anchors on the interfacial bond performance. The testing setup is shown in Figure 3 and a 50 mm unbonded region was reserved to avoid the edge effect [39]. The loading end of BFRP sheets was fixed and loaded by the testing machine and the applied load was recorded by an in-built load cell of the testing machine. The whole concrete block was fixed to the workbench by the designed steel jig to avoid any moment during the loading process. A digital camera was used to record the loading process and the successive images were obtained to carry out the digital image correlation (DIC) analysis.

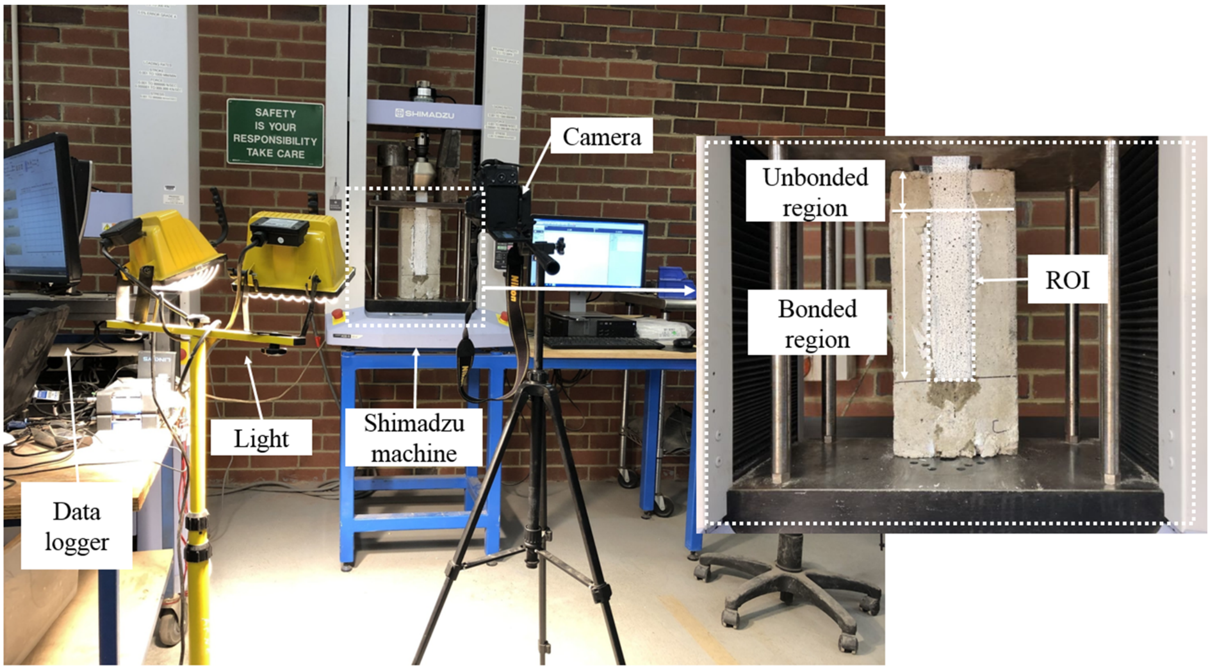

Figure 3. Test facilities and setup

4.1 Load and slip response

The load-slip curves at the loaded end are plotted in Figure 4. It is found that the ultimate debonding load and the ultimate slip increased in general with the diameter of epoxy anchors, indicating that using epoxy anchors enhanced the interfacial bond strength and delayed the debonding process. It can be observed that the load-slip curves of all the specimens changed slightly at approximately 4 kN, indicating that the micro-cracking initiated at the interface. Due to the existence of epoxy anchors, the difference of bonding behaviour was remarkable between the control specimen and the specimen with epoxy anchors. For the control specimens, the ultimate slip was around 1.60 mm on average. As shown in Figure 4 (b-g), the specimens with epoxy anchors experienced hardening behaviour before debonding which showed significantly enhanced ultimate debonding load and shear slip. The epoxy anchors enhanced the load-bearing capacity and ductility of the interface and thus increased the effective utilization of

BFRP sheets. The specimens with 15 mm diameter epoxy anchors showed the highest increment in both the bond strength and the ultimate shear slip. For the specimens D-15-3 with three anchors, the debonding load should be constant in the un-anchored area, but one of the test results shows a significant growth trend, which was caused by the thicker layer of adhesive near the last hole.

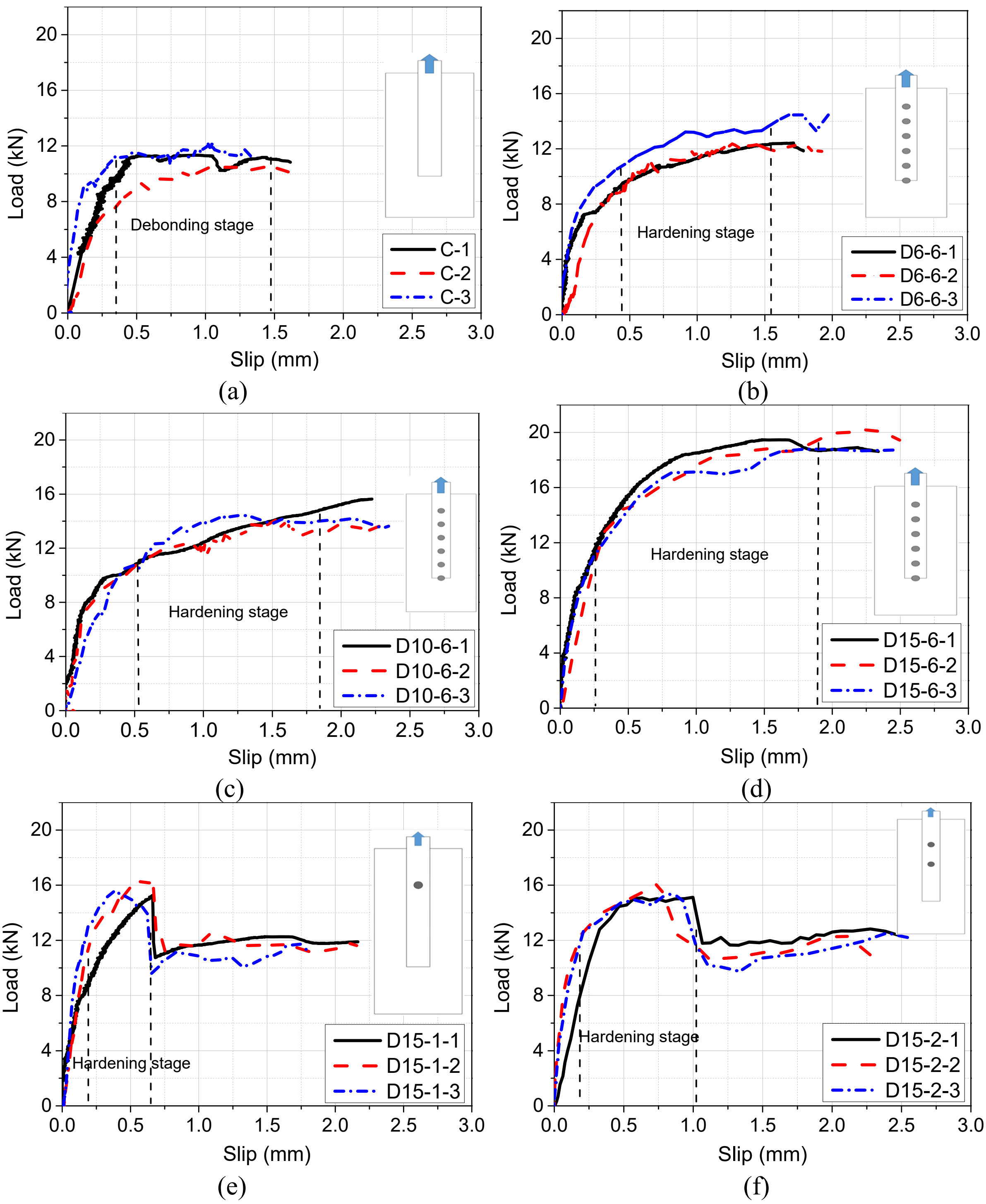

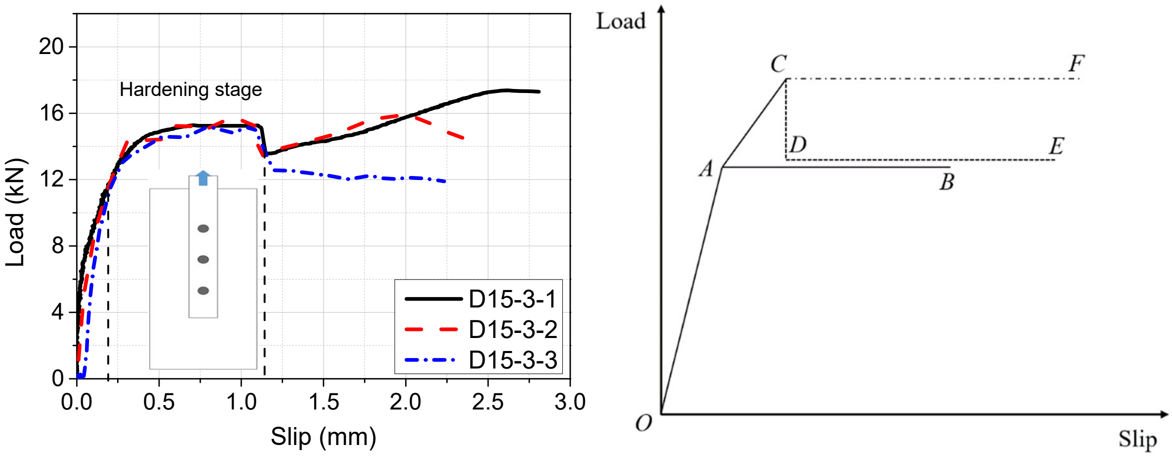

(g) (h)

Figure 4. Load and slip curves

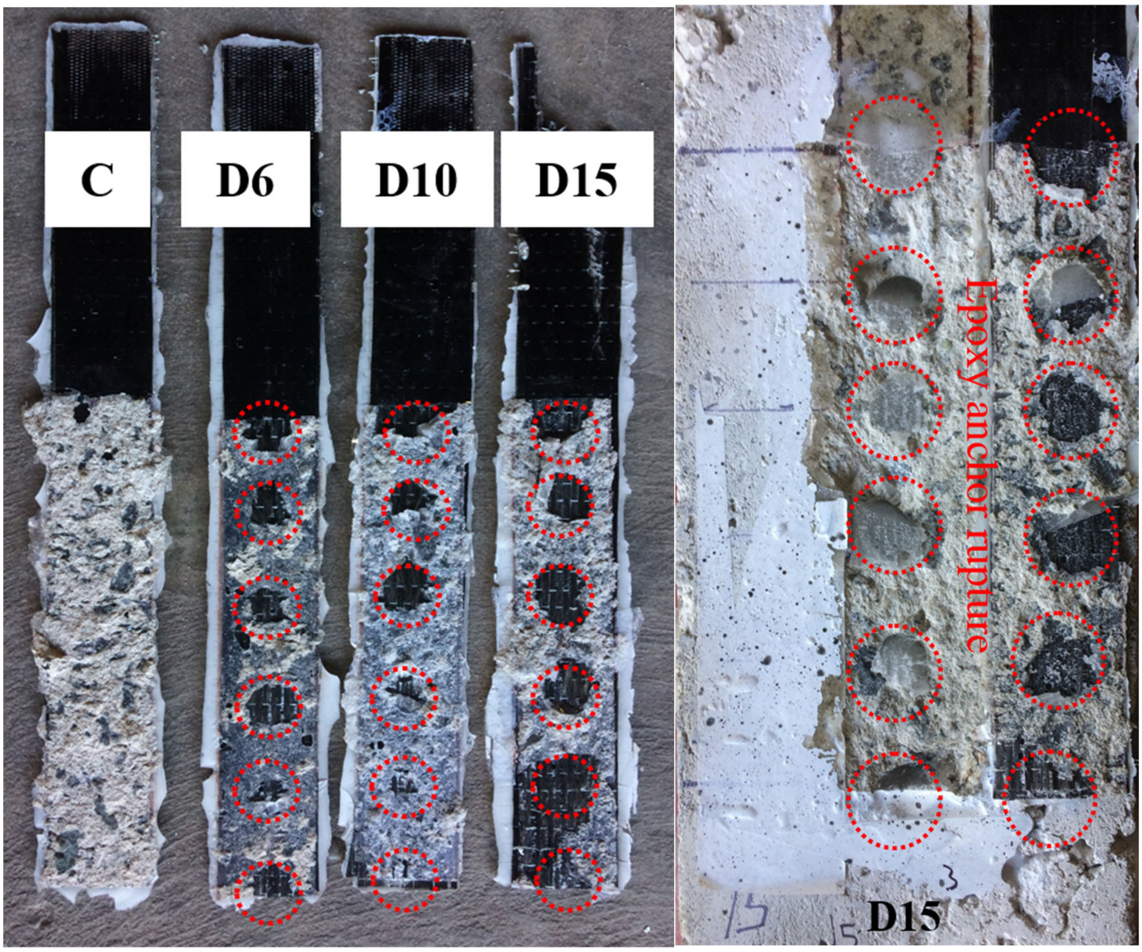

Figure 5. Fracture of epoxy anchors

To study the effect of the number of epoxy anchors on the bond performance, specimens D15-1 with one epoxy anchor, D15-2 with two epoxy anchors, D15-3 with three epoxy anchors, and D15-6 with six epoxy anchors were tested, the results are shown in Figure 4 (e-g), respectively.

It can be observed that the specimens with one, two, or three anchors exhibited different load-slip shapes as compared to the specimens with six anchors. The specimens with one, two, or three anchors showed a drop of the debonding load to a level similar to the debonding load of the reference specimen without anchor after the peak load, while the debonding load drop was not observed in specimens D15-6, in which the peak load was maintained up to a slip reaching about 2.5 mm in the test, indicating the greatly improved strength and slip due to sufficient anchors. Figure 4 (h) shows the simplified bond and slip curves proposed in the study based on the observations of test data. A generic load-slip curve for the control group (unanchored) can be expressed by the path O-A-B. The path O-A-C-F represents the generic behaviour of the specimens with sufficient anchors, i.e. six anchors, while the path O-A-C-D-E refers to the generic behaviour of the specimens with insufficient anchors or less than six anchors in this study (i.e. D15-1, D15-2 and D15-3). Stage OA refers to the load linearly increase up to the initial debonding load. After Point A, the debonding load of unanchored specimen is a constant determined by the bonding strength of concrete and FRP interface until FRP is fully detached from the concrete prism at Point B. The anchored specimen, however, has an increased debond load-carrying capacity after Point A, with the ultimate debonding load at Point C as shown in the figure. If the specimen has sufficient number of anchors, the debond load-carrying capacity after Point C remains constant until the final detachment at Point F owing to the total failure of anchors. For specimen with insufficient number of anchors, the load-carrying capacity drops to Point D and remains constant until the final detachment at Point E. The load level of Point D depends on the number of anchors. If there is only one anchor, the anchor failure makes the interface the same as the case without anchor, the load level then is the same as the reference case. If there are more than one anchor, the load level of Point D is slightly higher than that of the reference specimen. To quantify the enhancement of shear resistance of the anchored BFRP-to-concrete joints, the energy consumption (*EC*) of the BFRP-concrete interface which refers to the enclosed area of the load-slip curve is compared herein. The obtained *EC* is summarized in Table 1.

Figure 6 shows the effect of using epoxy anchors on the bonding behaviour of the BFRP-to-concrete interface. The general trend of the testing results shows that the average ultimate load, the ultimate shear slip, the ultimate debonding strain and the energy consumption increased remarkably with the diameter of epoxy anchor increasing from 6 mm to 15 mm. As compared to the control group, the increment of 19.23%, 33.89%, and 77.49% was obtained for the ultimate debonding load for specimens D6, D10, and D15, respectively. The ultimate slip increased by 25.05%, 50.77%, and 60.88%, respectively, while the ultimate debonding strain increased by 31.93%, 60.81%, and 86.71% for specimens with anchors of D6, D10, and D15, respectively. By virtue of epoxy anchors, more energy can be absorbed during the debonding process. The maximum energy consumption was 16.34 J and an increment of 143.28% was achieved for the specimens with 15 mm epoxy anchors as compared with the control group. Figure 6 (e) and (f) show the effect of the number of anchors on the ultimate debonding load and energy consumption. As shown in the load-slip curves in Figure 4, the specimens with insufficient anchors (i.e. D15-1, D15-2 and D15-3) and sufficient anchors showed similar ultimate debonding load and ultimate debonding strain, implying each anchor acts indepdently in resisting the debonding. This is because debonding initiates at the loaded end and propagates along the interface, before debonding reaches the particular anchor, its contribution to resist debonding is minimum. In general, the testing results showed that the embedded part of epoxy anchors led to a stronger bonding strength on the interface, which means higher strength efficiency of BFRP sheets was utilized.

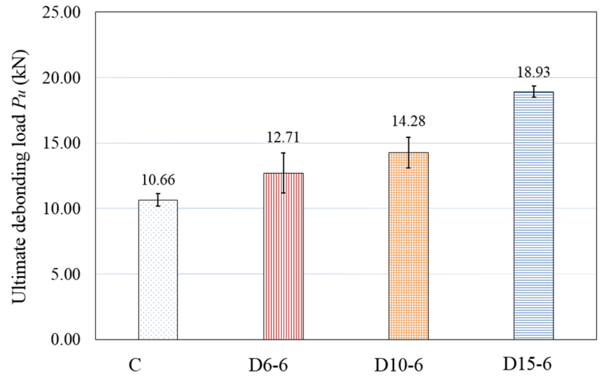

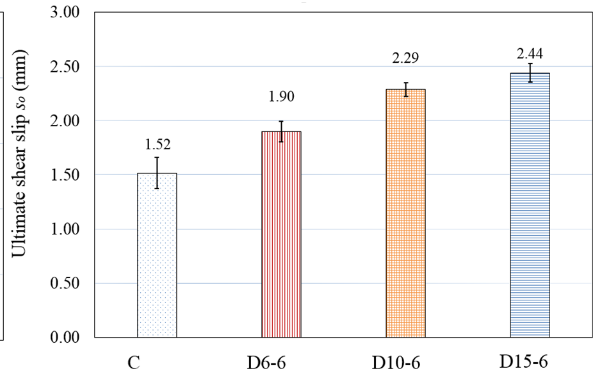

(a) Size effect on ultimate debonding load (b) Size effect ultimate shear slip

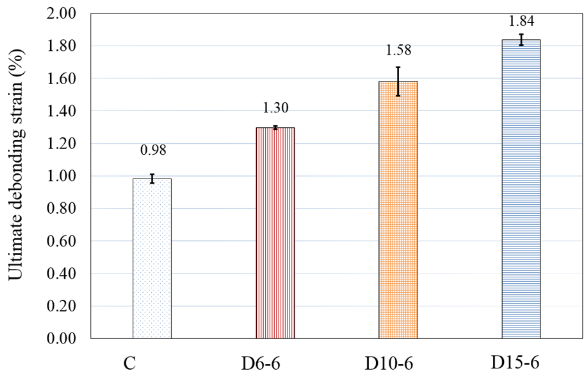

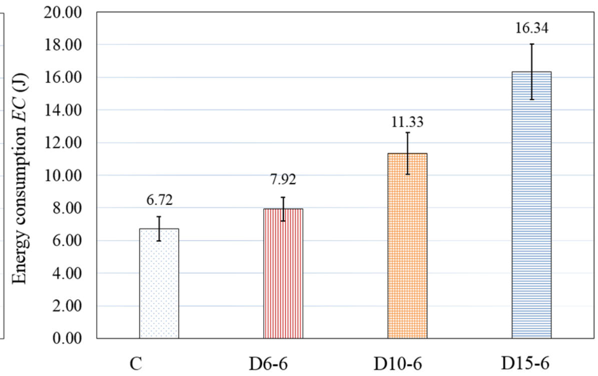

(c) Size effect ultimate debonding strain (d) Size effect energy consumption

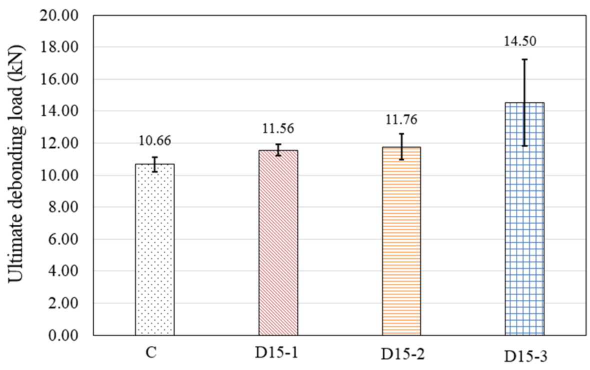

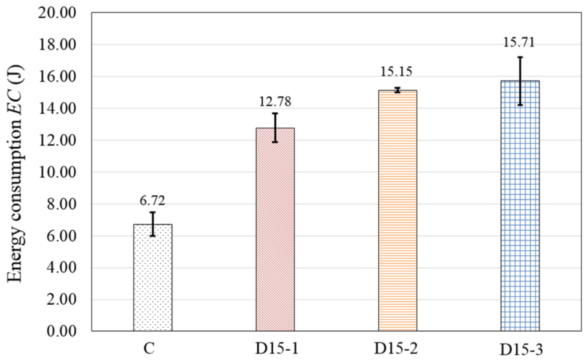

(e) Number effect ultimate debonding strain (f) Number effect energy consumption

Figure 6. Effect of size and number of epoxy anchor on bonding behaviour

Figure 7 illustrates the typical debonding failure modes after the detachment. The debonding failure initiated in the concrete layer with a flake of concrete pulling out from the concrete substrate. It was found that the thickness of damaged concrete for the specimens with epoxy anchors (e.g. D15-1) was thinner than the control group. The decreased concrete damage thickness was caused by the shifted debonding failure mode. For the control group without any anchors, the shear stress penetrated through the weakest concrete layer and consequently damaged the concrete layer, where the shear stress changed into tensile stress in an angle of

45° [40]. Therefore, the debonding initiated on the tensile side of concrete element. However, for the specimens with epoxy anchors, the cracking resistance of concrete near the epoxy anchors was enhanced and consequently the debonding failure shifted to the interface between adhesive and concrete. Meanwhile, the fracture of epoxy anchors was observed at the interface between adhesive and concrete, indicating that the embedment depth of 20 mm was sufficient for the epoxy anchors and consequently a strong dowel action was achieved.

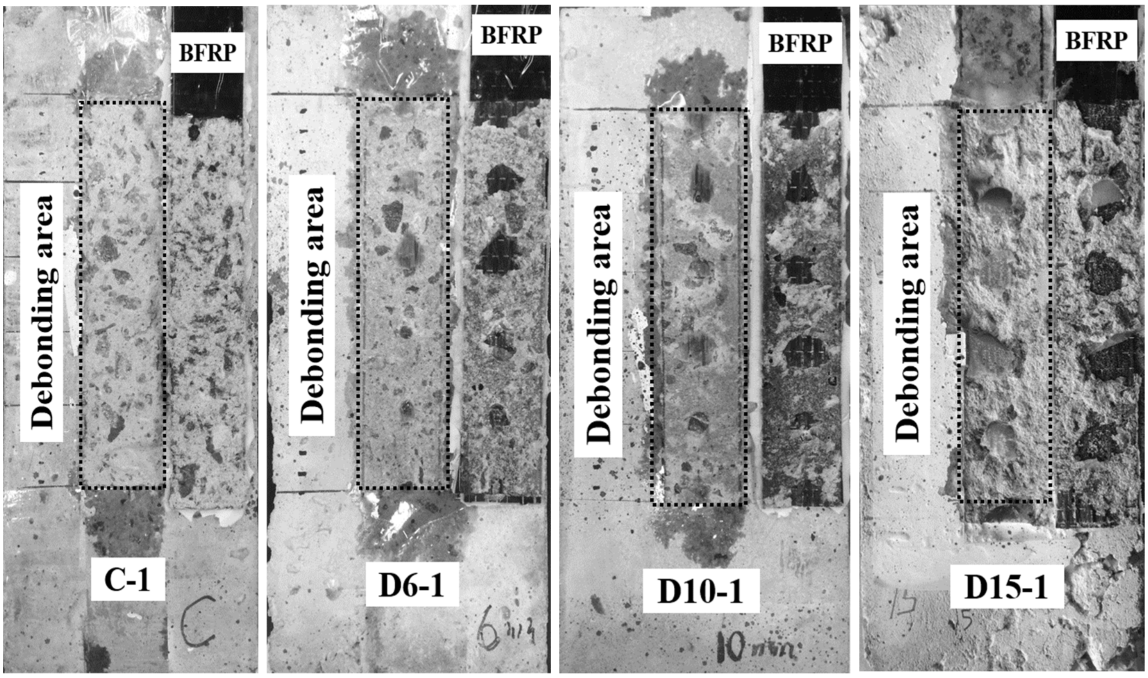

Figure 7. Typical debonding failure modes

Figure 8 illustrates the enhancement mechanism of using epoxy anchors. For the control specimens without anchors, the cracks penetrated through the concrete tensile side as the tensile strength of concrete (i.e. 3.9 MPa) was much lower than that of epoxy resin (i.e. 50 MPa). However, for the specimens with epoxy anchors, the interlocking action between epoxy anchors and concrete enhanced due to the effective embedment depth of epoxy anchors and consequently the epoxy anchors failed at the interface of the BFRP and epoxy resin. As epoxy anchors were arranged within the effective bond length (i.e. 40 mm), the consistent improvement in the shear stress transfer was achieved which can be verified in the load-slip response.

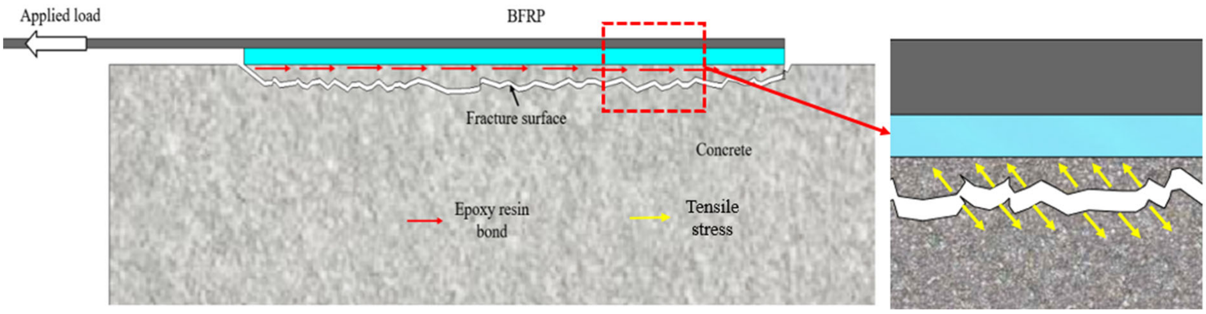

(a) Unanchored specimen

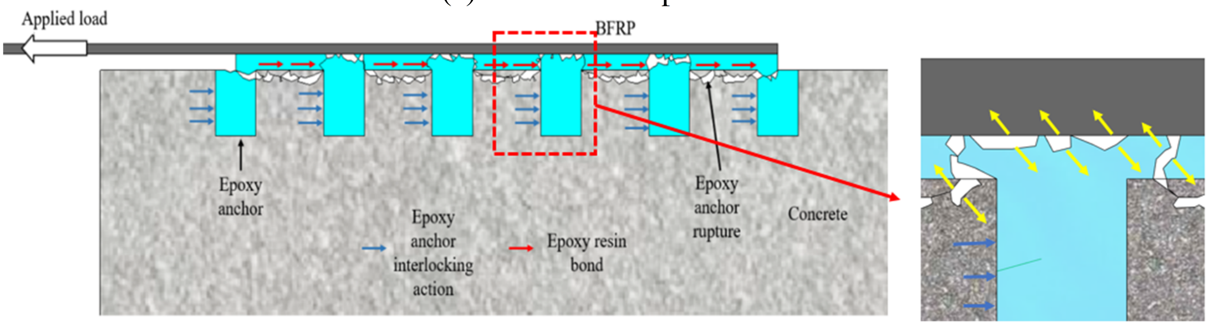

(b) Multiple-anchored specimen

Figure 8. Debonding mechanism with and without epoxy anchor

4.2 Strain distributions

The DIC technique was used to measure the BFRP strain and the accuracy of this non-contact technique was carefully validated in the previous studies by the authors to achieve reliable test data [9, 41]. The typical strain distributions along the BFRP sheets are plotted in Figure 9 (a-d). Four different loading levels (P_2, P_3, P_4 and P_5) after the initial debonding stage (P_1) were selected to present the strain distributions in the debonding process. The difference between the anchored and un-anchored specimens is the initial debonding stage and final debonding stage, which are marked as red circles in Figure 9. For the control specimens, the debonding strain at the initial debonding stage (0.79%) was close to that at the final debonding stage (0.98%). For the anchored specimens (i.e., D6-6, D10-6 and D15-6), the debonding strain increased more significantly from the initial debonding stage to final debonding stage as compared to the un-anchored specimens. For instance, the debonding strain increased from

1.19% at the initial debonding stage to 1.74% at the final debonding stage for specimen D15-6 owing to the existence of interfacial hardening stage.

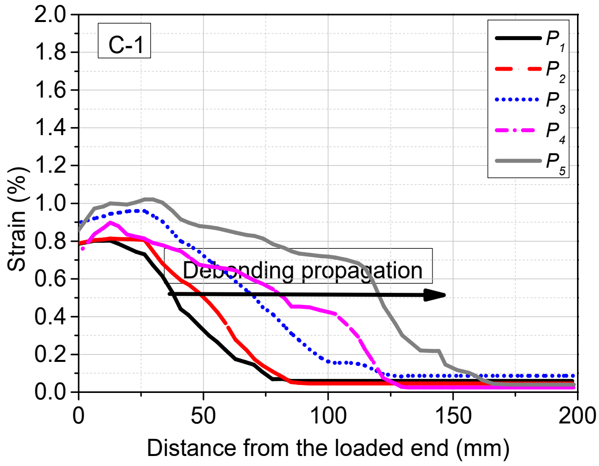

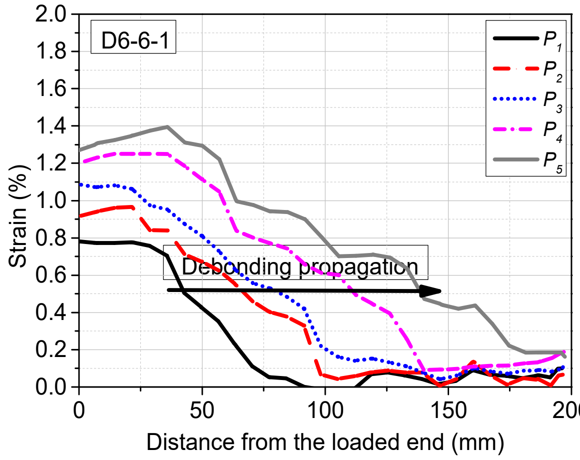

(a) C-1 (b) D6-6-1

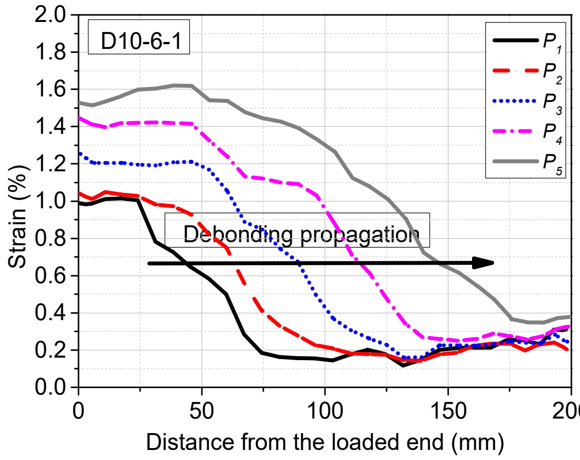

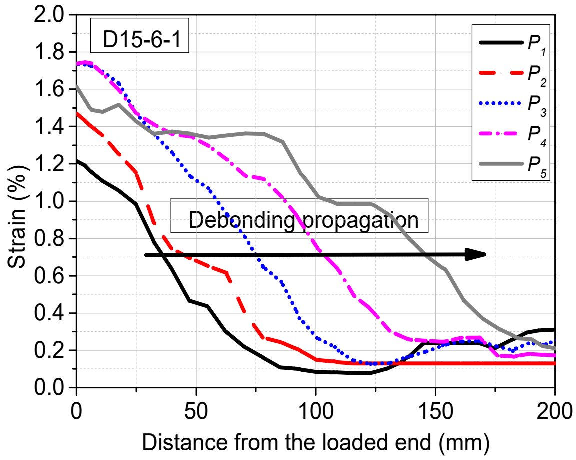

(c) D10-6-1 (d) D15-6-1

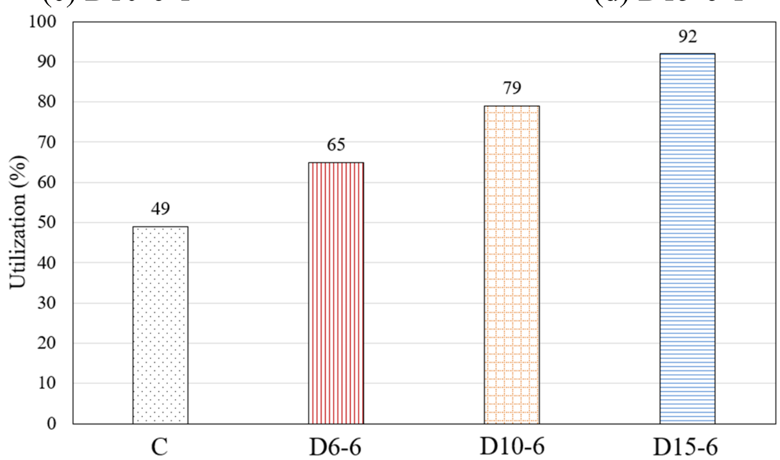

(e) Utilization of rupture strain capacity of BFRP sheet

Figure 9. BFRP strain distribution and utilization rate

Figure 9 (e) illustrates the utilization of rupture strain capacity of BFRP sheets (i.e. strain utilization), which is defined as the ratio of its maximum debonding strain and ultimate rupture strain. The ultimate rupture strain of BFRP sheets was obtained from the coupon tensile tests. The maximum debonding strain increased from 0.98% to 1.80% on average as compared to the control specimen. The strain utilization of BFRP sheets on average increased from 49% to 92% as compared to the control specimen. This enhancement was dependent on the increased size of epoxy anchors, i.e., the increase of the anchorage area. It should be noted that this enhancement can only be achieved by continuously increasing the anchor size within the effective bond length. Therefore, the epoxy anchors can improve the utilization efficacy of the strengthening materials.

4.3 Effective shear stress transfer length

Figure 10 illustrates the initial debonding stage of the tested specimens. The specimens with epoxy anchors did not show a significant initial debonding stage as compared to the control specimen C-1. After the initial debonding stage at approximately 290 s, the control specimen C-1 showed a significant loading plateau before the final detachment. At the initial debonding stage, the shear stress transfer length of specimen C-1was around 50 mm, as shown in the strain contour graph in Figure 10, which can be also defined as the effective bond length (EBL). Previous studies [10, 42] have reported that the EBL is the active bond zone, over which the extension of bond length has no effect on debonding capacity. As shown in Figure 10, the strain contours consisting of red, yellow, green, light blue and dark blue colours refer to the shear stress transfer length at the initial debonding stage. Since the initial debonding stage coincided with the final detachment of the specimens with epoxy anchors due to the hardening behaviour, it is collectively named as the debonding stage for all the specimens with epoxy anchors. According to the strain contours, the EBL increased remarkably due to the anchorage effect. For the specimens with sufficient anchors, the EBL was approximately 200 mm which was close to the entire bonding length, indicating that the existence of epoxy anchors not only extended the stress transfer length, but also prolonged the duration of debonding.

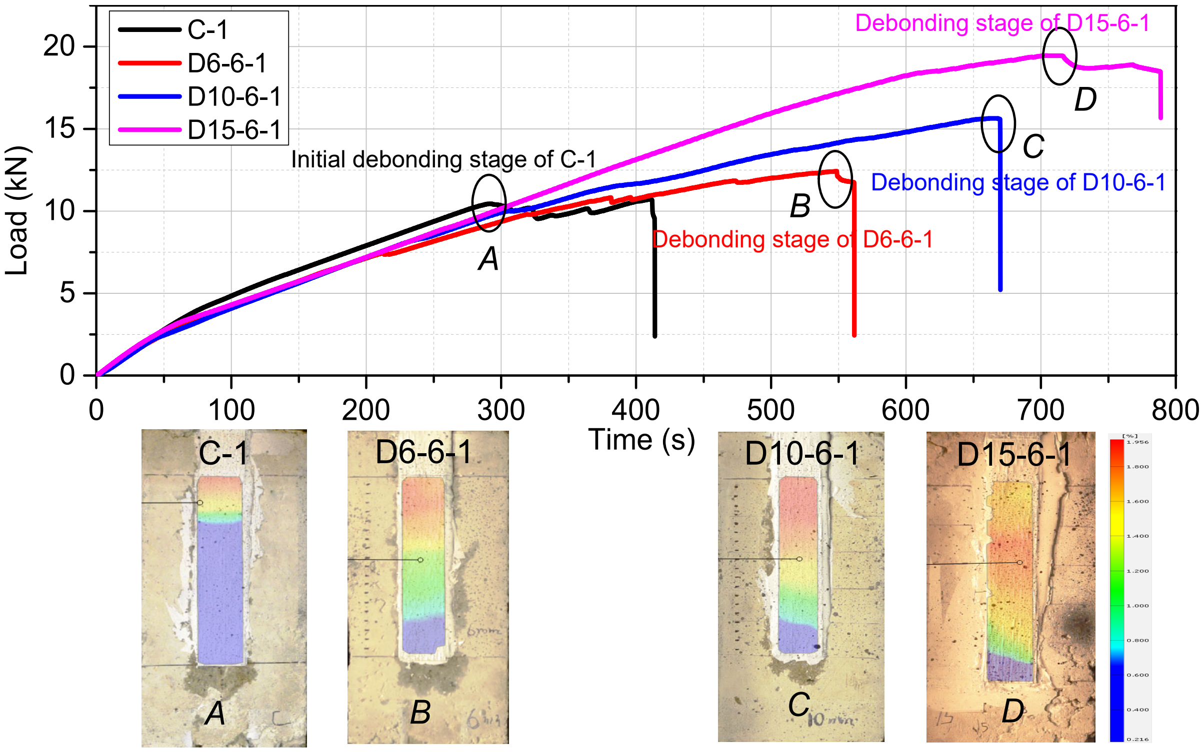

Figure 10. Debonding load and effective bond length (EBL)

4.4 Shear stress and slip response

Figure 11 shows the relationship between shear stress and slip of the tested specimens. The shear stress and slip were obtained using Equations (1) and (2) [43, 44], as below

$$s(x) = \int_0^{\infty} \varepsilon dx \qquad (1)$$

$$\tau(x) = \frac{d\varepsilon}{dx} E_f t_f \qquad (2)$$

in which E_f is the elastic modulus of BFRP sheets, t_f is the nominal thickness of BFRP sheets, and ε is the strain along BFRP sheets. The general trend shows that the peak shear stress increased with the addition of epoxy anchors. To obtain more accurate and consistent bond-slip responses, at least four loading stages (i.e. P_1, P_2, P_3 and P_4) were selected. The experimental bond-slip curves showed the fluctuations due to the non-uniformity of concrete surface. To eliminate the impact of data fluctuations and obtain the average shear stress, an analytical regression equation proposed by the previous studies [45-47] was also adopted in this study, which can be expressed as $\tau(s) = \frac{E_f t_f \alpha}{\beta^2} e^{-\frac{s}{\alpha}} \left(1 - e^{-\frac{s}{\alpha}}\right)$, where α and β are the fitting coefficients given in Table 1. It should be noted that the bond-slip response of specimen D15-6-1 shows a different profile after the softening stage as compared to the other specimens, which is due to the residual stress caused by the rupture of epoxy resin. The residual stress increased with the anchor size.

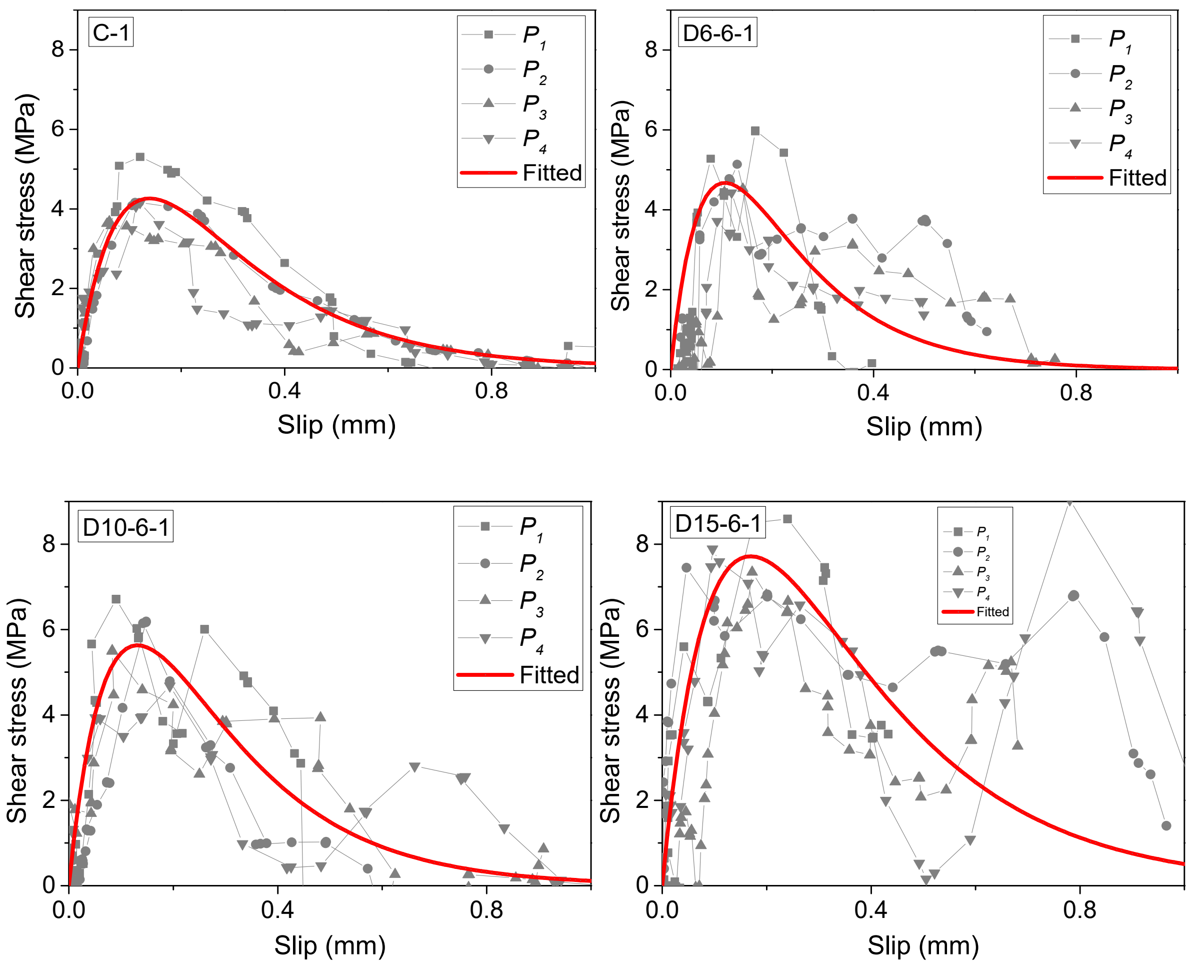

Figure 11. Bond-slip response

5. Analytical study on the effect of epoxy anchors

5.1 Simplified load-strain response

To quantify the contribution of epoxy anchors on the interfacial bond strength, the debonding load at different loading stages can be predicted using strain of BFRP sheets. Based on the derived load-strain relationships, a simplified model is suggested for the specimens with or without sufficient epoxy anchors. It should be noted that the micro-cracking stage induced by concrete cracking was neglected for ease of comparison. As shown in Figure 12 (e), two main stages (i.e. elastic stage and debonding stage) were observed for the control group, and three main stages (i.e. elastic stage, hardening stage and debonding stage) were observed for the specimens with epoxy anchors. The power function of $P = \lambda_1 \varepsilon^{\lambda_2}$ was used to describe the non-linear stage (i.e. hardening stage), in which *P* is the debonding load, *ε* is the FRP strain and the parameters $\lambda_1 = 11.25$ and $\lambda_2 = 0.20$ are fitting coefficients derived from the experimental results. Compared with the control group, the specimens with epoxy anchors exhibited the hardening stage, which greatly enhanced both the interfacial bond strength and ductility. Due to different cross-sectional areas of epoxy resin anchors, the level of enhancement varied with the sizes of epoxy anchors.

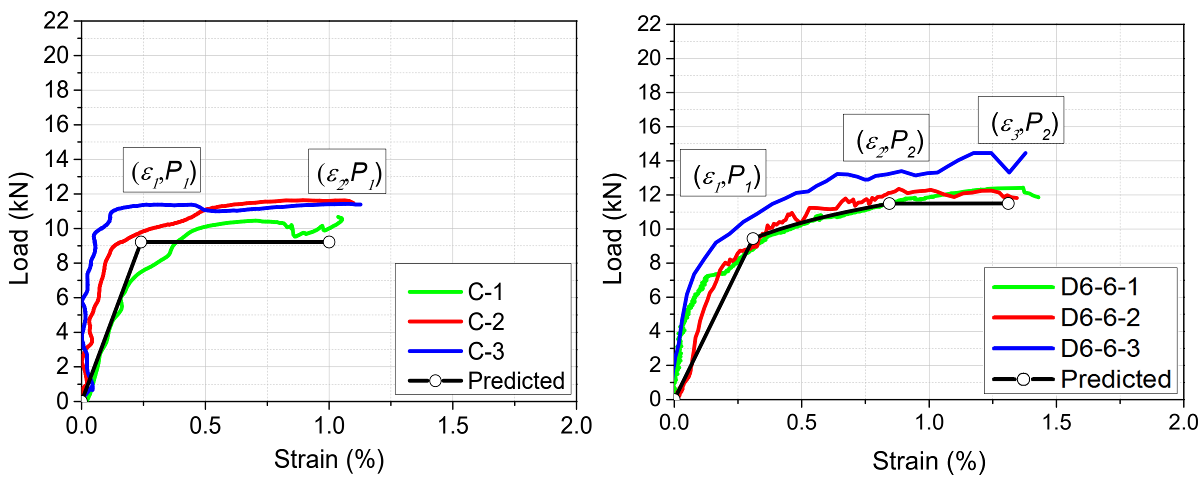

(a) Control group (b) D6

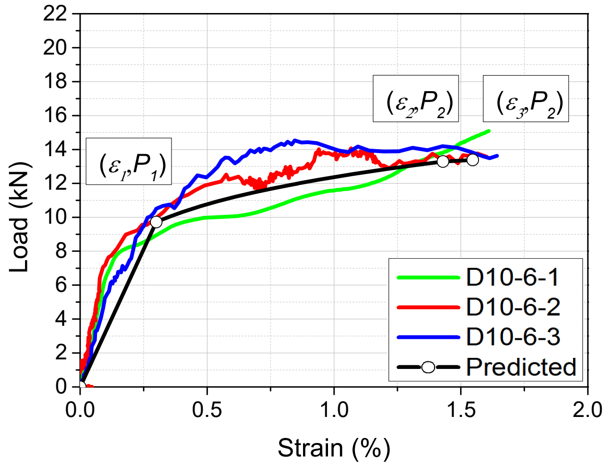

(c) D10

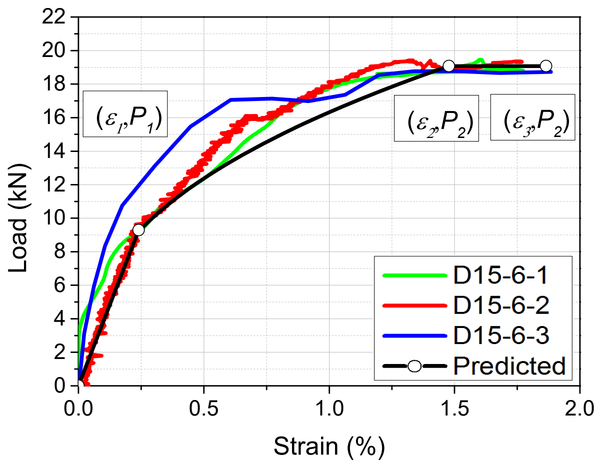

(d) D15

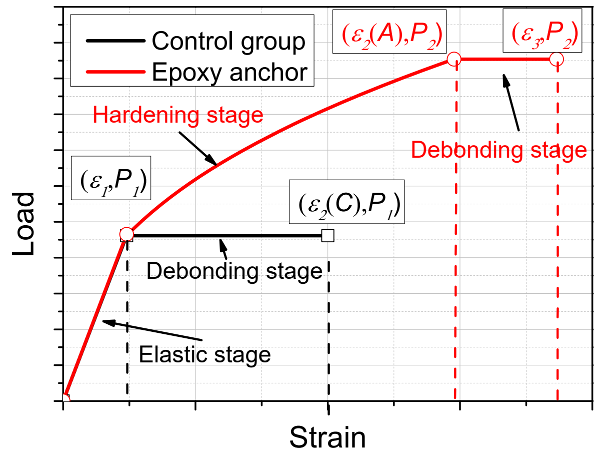

(e) Comparison between control group and anchorage group

Figure 12. Load-strain responses

5.2 Shear stress distribution

Figure 13 shows the shear stress distributions along the bond area. Compared with the control group, the specimens with epoxy anchors exhibited a higher bond strength due to the dowel action from the embedded epoxy resin anchors. Based on the predicted debonding loads at different loading stages, the corresponding strain can be obtained. By integrating the strain along the bond length, the shear slip can be obtained accordingly. The strain distribution of BFRP sheets within the effective bond length can be expressed as follows:

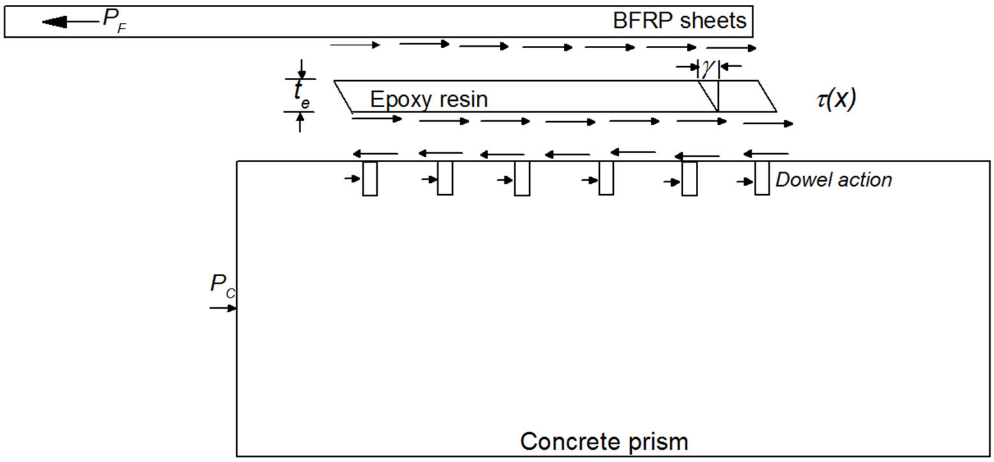

Figure 13. Shear stress distributions

$$\varepsilon_F(x) = \frac{Pi}{bE_F t_F} \frac{\sinh\left[\phi(L_e - x)\right]}{\sinh(\phi L_e)} \tag{3}$$

with $\phi^2 = \left(\frac{G_A}{t_A} \frac{1}{E_F t_F} \left(1 + \frac{E_F A_F}{E_C A_C} \right) \right)$.

The interfacial fracture energy G_f can be defined as the enclosed area under the bond-slip curve, which can be expressed as follows:

$$G_f = \int_0^{Le} \tau(x) ds \tag{4}$$

with $ds = \frac{t_A}{G_A} d\tau(x)$

$$G_f = \frac{1}{2} \frac{Pi^2}{b^2 E_F t_F} \left(1 + \frac{E_F A_F}{E_C A_C} \right) \tag{5}$$

in which Pi is the load at different stages, ε_F refers to BFRP strain at different loading stages, b is the bonding width of BFRP sheet, $E_f t_f$ is the BFRP stiffness, G_A is the shear modulus of epoxy resin, and t_A is the thickness of epoxy resin. The debonding loads of the two stages need to be determined first, followed by the corresponding strain. The bond strength model proposed by Chen and Teng [48] was used to predict the bonding load P as the accuracy of this model has been verified in the previous studies [9, 49]. Therefore, the bonding load P_1 at the elastic stage can be determined by Equation (6).

$$P_1 = 0.427 k_w b_f L_e \sqrt{f_c} \tag{6}$$

in which $k_w = \sqrt{\dfrac{2 - b_f / b_c}{1 + b_f / b_c}}$ and $L_e = \sqrt{\dfrac{E_f t_f}{\sqrt{f_c}}}$.

For the specimens with epoxy anchors, the initial debonding load increased with the size of epoxy anchors (d_e). As fracture of epoxy anchors was observed for all the specimens with anchors, the strain energy ($\dfrac{f_e^2}{2E_e}$) and bonding area (A_e) of epoxy anchors should be also the factors for determining the interfacial bond strength. Therefore, the initial debonding load P_2 at the hardening stage can be determined by the following equation:

$$P_2 = P_1 + \alpha_1 d_e \left(\frac{f_e^2}{2E_e} A_e \right)^{\alpha_2} \tag{7}$$

in which P_1 is the bonding strength of the elastic stage, P_2 is the bonding strength of the hardening stage and α_1 and α_2 are the fitting coefficients. The best-fitted results are plotted in Figure 14. The derived bonding strength P_1 from Equation (6) was 9.22 kN and the regressed coefficients α_1 and α_2 were 0.59 and 0.18, respectively. Therefore, the following equation can be obtained by substituting these coefficients into Equation (7):

$$P_2 = P_1 + 0.59 d_e \left(\frac{f_e^2}{2E_e} A_e \right)^{0.18} \tag{8}$$

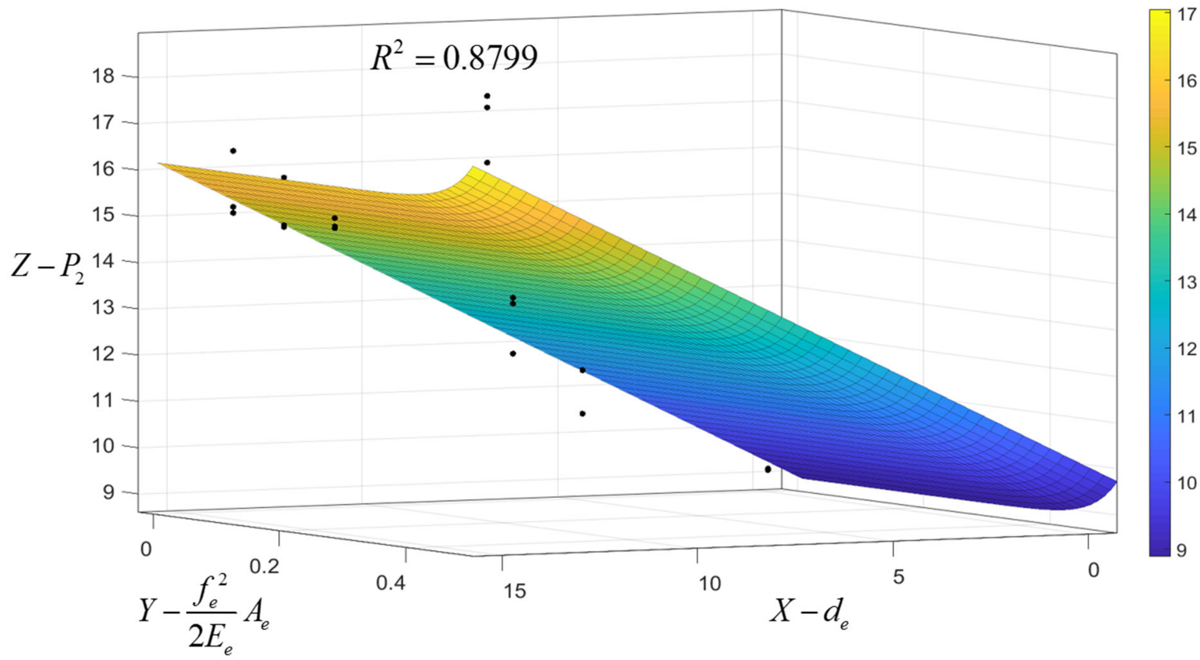

Figure 14. Regression analysis of bond strength P_2

Figure 15 shows the comparison between the predicted and tested bond strength of P_1 and P_2. It is observed that the analytical results match well with the experimental data with a high correlation coefficient R^2=0.87, indicating that the proposed analytical bond strength model by incorporating the effect of epoxy anchors yields good prediction.

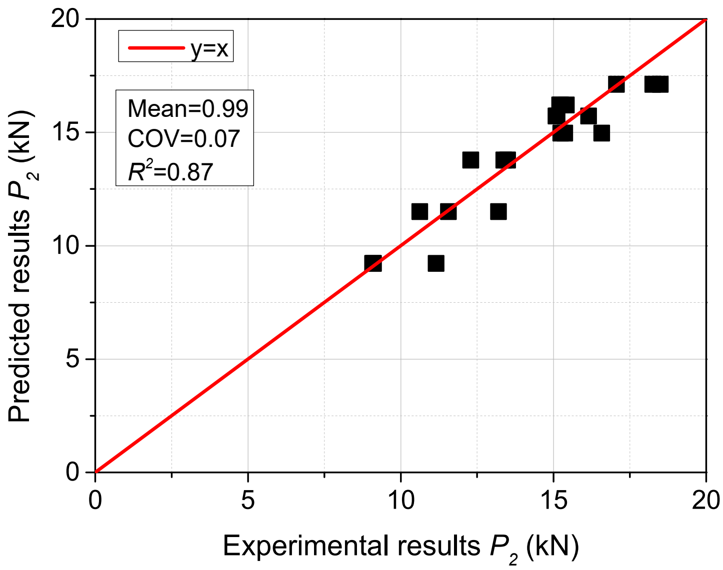

Figure 15. Comparison between the predicted and experimental results P_2

5.3 Debonding load

Based on the typical simplified load-strain curves, the bond strength P_1 can be obtained for all the tested specimens based on the analytical models proposed in this study. Based on the derived bond strength P_1 from Equation (6), the elastic debonding strain ε_1 can be expressed as:

$$\varepsilon_1 = \frac{P_1}{bE_F t_F} \frac{\sinh\left[\phi\left(L_e - x\right)\right]}{\sinh\left(\phi L_e\right)} \tag{9}$$

For the specimens without epoxy anchors, after the initial debonding stage the BFRP-to-concrete interface maintained the same debonding load P_1 until the final detachment. The tensile strain ε_2 can be determined by the derived bond strength P_1, as shown in the following equation:

$$\varepsilon_{2(C)} = \frac{P_1}{b_f E_F t_F} \tag{10}$$

in which P_1 is the bond strength at the elastic stage, $\varepsilon_{2(C)}$ is the ultimate debonding strain of the control group, L_e is the effective bond length and x is the distance from the loaded end.

For the specimens with epoxy anchors, the interface continued to carry higher loads after the elastic stage due to the existence of epoxy anchors. The BFRP sheets continued to be subjected to the interfacial bond strength provided by the epoxy anchors and the corresponding strain ε_2 can be predicted by the bond strength P_2 at the hardening stage, as shown in the following equation:

$$\varepsilon_{2(A)} = \frac{P_2}{bE_F t_F} \frac{\sinh\left[\phi\left(L_e - x\right)\right]}{\sinh\left(\phi L_e\right)} \tag{11}$$

in which P_2 is the initial debonding load for the specimens with epoxy anchors and $\varepsilon_{2(A)}$ is the initial debonding strain for the specimens with epoxy anchors. Once the debonding initiated, the BFRP sheets are only subjected to tensile force without any bonding after the epoxy resin hardening. The elongation of BFRP at the debonding plateau ε_3 can be determined by the sum of the elastic debonding strain ε_1 and the initial debonding strain $\varepsilon_{2(A)}$, as shown in the following equation:

$$\varepsilon_3 = \varepsilon_{2(A)} + \varepsilon_1 \tag{12}$$

The predicted bond strength P_1 and P_2 and the corresponding strain ε_1, $\varepsilon_{2(C)}$, $\varepsilon_{2(A)}$ and ε_3 are summarized in Table 2. It should be noted that x is the position of the selected point from the loaded end. The predicted results are plotted in Figure 16. It is observed that the bond strength and the ultimate debonding strain increased with the rising anchorage area, which is consistent with the experimental results.

Table 2. Comparison of predicted results and experimental results

Specimen ID	$P_{1,exp.}$ (kN)	$P_{1,pre.}$ (kN)	$P_{2,exp.}$ (kN)	$P_{2,pre.}$ (kN)	$\varepsilon_{1,pre.}$ (%)	$\varepsilon_{2,exp.}$ (%)	$\varepsilon_{2,pre.}$ (%)	$\varepsilon_{3,pre.}$ (%)
C	9.78	9.22	9.78	9.22	0.236	0.983	0.877	/
D6	9.50	9.22	11.79	11.50	0.236	1.297	1.094	1.330
D10	10.15	9.22	13.05	13.78	0.236	1.581	1.311	1.547
D15	11.37	9.22	17.94	17.12	0.236	1.836	1.629	1.865

Note: $P_{i,exp}$ and $\varepsilon_{i,exp}$ refer to the average experimental results and $P_{i,pre}$ and $\varepsilon_{i,pre}$ refer to the predicted results.

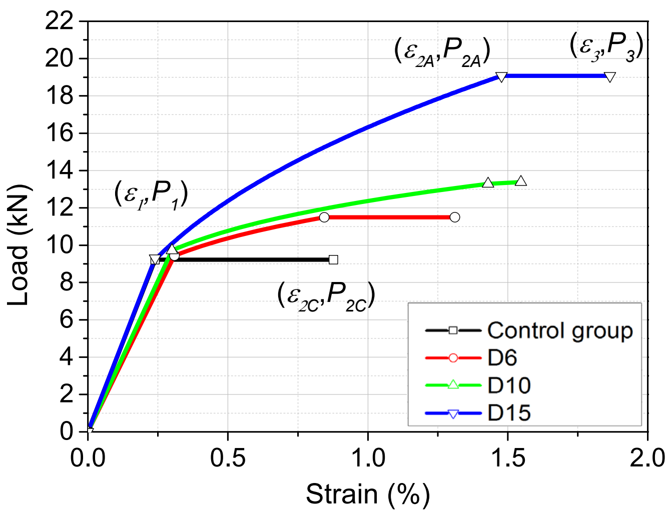

Figure 16. Predicted debonding load and strain

6. Conclusion

In the present study, a new epoxy anchor system was developed to enhance the interfacial bond performance between BFRP sheets and concrete. As compared to the existing anchors, the newly proposed epoxy anchor system was easy to implement for engineering practice and required less workmanship. The embedded part of the epoxy anchor in the concrete formed self-anchorage to enhance the interfacial shear resistance. The experimental results showed 77.49% increment in bond strength, 86.71% increment in the utilization of BFRP sheet, and 78.10% increase in the peak shear stress on average. The size of epoxy anchors significantly affected the shear resistance. Increasing the diameter of epoxy anchor greatly enhanced the shear resistance while the peak bond strength and peak shear stress were not affected by the number of epoxy anchors in general. In addition, an analytical bond strength model was proposed by incorporating the bonding area and strain energy of epoxy resin and it showed a good agreement with the testing results. With the analytical bond strength model, the FRP strain at different loading stages can be also predicted.

Acknowledgement

The authors thank the Australian Research Council (ARC LP150100259) for its financial support.

Compliance with ethical standards

Conflict of interest

The authors declare that they have no conflict of interest.

References

[1] W. Chen, T.M. Pham, H. Sichembe, L. Chen, H. Hao. Experimental Study of Flexural Behaviour of Rc Beams Strengthened by Longitudinal and U-Shaped Basalt Frp Sheet. Compos B Eng 134 (2018) 114-26.

[2] J.-F. Jiang, Y.-F. Wu. Plasticity-Based Criterion for Confinement Design of Frp Jacketed Concrete Columns. Materials and Structures 49 (6) (2016) 2035-51.

[3] C. Yuan, W. Chen, T.M. Pham, H. Hao. Bond Behavior between Basalt Fibres Reinforced Polymer Sheets and Steel Fibres Reinforced Concrete. Eng Struct 176 (2018) 812-24.
[4] C. Yuan, W. Chen, T.M. Pham, L. Chen, J. Cui, Y. Shi, H. Hao. Effect of Aggregate Size on the Dynamic Interfacial Bond Behaviour between Basalt Fiber Reinforced Polymer Sheets and Concrete. Constr Build Mater 227 (2019a) 116584.
[5] T.C. Rousakis, A.I. Karabinis. Adequately Frp Confined Reinforced Concrete Columns under Axial Compressive Monotonic or Cyclic Loading. Materials and structures 45 (7) (2012) 957-75.
[6] C. Jiang, B. Wan, Y.-F. Wu, J. Omboko. Epoxy Interlocking: A Novel Approach to Enhance Frp-to-Concrete Bond Behavior. Constr Build Mater 193 (2018) 643-53.
[7] J. Cromwell, K. Harries, B. Shahrooz. Environmental Durability of Externally Bonded Frp Materials Intended for Repair of Concrete Structures. Constr Build Mater 25 (5) (2011) 2528-39.
[8] C. Yuan, W. Chen, T.M. Pham, H. Hao, J. Cui, Y. Shi. Strain Rate Effect on Interfacial Bond Behaviour between Bfrp Sheets and Steel Fibre Reinforced Concrete. Compos B Eng (2019d) 107032.
[9] C. Yuan, W. Chen, T.M. Pham, H. Hao. Bond Behaviour between Hybrid Fiber Reinforced Polymer Sheets and Concrete. Constr Build Mater 210 (2019b) 93-110.
[10] J.F. Chen, J. Teng. Anchorage Strength Models for Frp and Steel Plates Bonded to Concrete. J Struct Eng 127 (7) (2001) 784-91.
[11] S.T. Smith, J. Teng. Frp-Strengthened Rc Beams. I: Review of Debonding Strength Models. Eng Struct 24 (4) (2002) 385-95.
[12] S.V. Grelle, L.H. Sneed. Review of Anchorage Systems for Externally Bonded Frp Laminates. Int J Concr Struct M 7 (1) (2013) 17-33.
[13] U. Ebead, H. Saeed. Frp/Stirrups Interaction of Shear-Strengthened Beams. Materials and Structures 50 (2) (2017) 103.
[14] H. Zhang, S.T. Smith. Influence of Plate Length and Anchor Position on Frp-to-Concrete Joints Anchored with Frp Anchors. Compos Struct 159 (2017) 615-24.
[15] T. Ozbakkaloglu, M. Saatcioglu. Tensile Behavior of Frp Anchors in Concrete. J Compos Constr 13 (2) (2009) 82-92.
[16] H. Zhang, S.T. Smith, R.J. Gravina, Z. Wang. Modelling of Frp-Concrete Bonded Interfaces Containing Frp Anchors. Constr Build Mater 139 (2017) 394-402.
[17] R. Kalfat, R. Al-Mahaidi, S.T. Smith. Anchorage Devices Used to Improve the Performance of Reinforced Concrete Beams Retrofitted with Frp Composites: State-of-the-Art Review. J Compos Constr 17 (1) (2011) 14-33.
[18] B. Fu, J.G. Teng, J.F. Chen, G.M. Chen, Y.C. Guo. Concrete Cover Separation in Frp-Plated Rc Beams: Mitigation Using Frp U-Jackets. J Compos Constr 21 (2) (2016) 04016077.
[19] Y.-F. Wu, Y. Huang. Hybrid Bonding of Frp to Reinforced Concrete Structures. J Compos Constr 12 (3) (2008) 266-73.
[20] F.G. Carozzi, P. Colombi, G. Fava, C. Poggi. Mechanical and Bond Properties of Frp Anchor Spikes in Concrete and Masonry Blocks. Compos Struct 183 (2018) 185-98.
[21] Y.-F. Wu, L. He, L. Bank. Bond-Test Protocol for Plate-to-Concrete Interface Involving All Mechanisms. J Compos Constr 20 (1) (2015) 04015022.
[22] G. Spadea, F. Bencardino, R. Swamy. Structural Behavior of Composite Rc Beams with Externally Bonded Cfrp. J Compos Constr 2 (3) (1998) 132-7.
[23] W. Sun, H. Liu, Y. Wang, T. He. Impacts of Configurations on the Strength of Frp Anchors. Compos Struct 194 (2018) 126-35.
[24] H. Zhang, S.T. Smith, S. Kim. Optimisation of Carbon and Glass Frp Anchor Design. Constr Build Mater 32 (2012) 1-12.

[25] K.K. Antoniades, T.N. Salonikios, A.J. Kappos. Cyclic Tests on Seismically Damaged Reinforced Concrete Walls Strengthened Using Fiber-Reinforced Polymer Reinforcement. ACI Struct J 100 (4) (2003) 510-8.
[26] H. Toutanji, G. Ortiz. The Effect of Surface Preparation on the Bond Interface between Frp Sheets and Concrete Members. Compos Struct 53 (4) (2001) 457-62.
[27] M. Mohammadi, D. Mostofinejad, M. Barghian. Effects of Surface Preparation Method on Frp-Concrete Bond Strength under Alkaline Conditions. J Compos Constr 21 (4) (2017) 04017010.
[28] I. Iovinella, A. Prota, C. Mazzotti. Influence of Surface Roughness on the Bond of Frp Laminates to Concrete. Constr Build Mater 40 (2013) 533-42.
[29] A. Hosseini, D. Mostofinejad. Effect of Groove Characteristics on Cfrp-to-Concrete Bond Behavior of Ebrog Joints: Experimental Study Using Particle Image Velocimetry (Piv). Constr Build Mater 49 (2013) 364-73.
[30] A. Hosseini, D. Mostofinejad. Experimental Investigation into Bond Behavior of Cfrp Sheets Attached to Concrete Using Ebr and Ebrog Techniques. Compos B Eng 51 (2013) 130-9.
[31] L. De Lorenzis, J. Teng. Near-Surface Mounted Frp Reinforcement: An Emerging Technique for Strengthening Structures. Compos B Eng 38 (2) (2007) 119-43.
[32] S. Zhang, J. Teng, T. Yu. Bond–Slip Model for Cfrp Strips near-Surface Mounted to Concrete. Eng Struct 56 (2013) 945-53.
[33] S. Zhang, J. Teng. End Cover Separation in Rc Beams Strengthened in Flexure with Bonded Frp Reinforcement: Simplified Finite Element Approach. Materials and Structures 49 (6) (2016) 2223-36.
[34] A. Committee. Guide for the Design and Construction of Externally Bonded Frp Systems for Strengthening Concrete Structures (Aci 440.2 R-17). Farmington Hills, MI: Author (2008).
[35] D. Mostofinejad, S.M. Shameli. Externally Bonded Reinforcement in Grooves (Ebrig) Technique to Postpone Debonding of Frp Sheets in Strengthened Concrete Beams. Constr Build Mater 38 (2013) 751-8.
[36] D. Mostofinejad, M.H. Mofrad, A. Hosseini, H.H. Mofrad. Investigating the Effects of Concrete Compressive Strength, Cfrp Thickness and Groove Depth on Cfrp-Concrete Bond Strength of Ebrog Joints. Constr Build Mater 189 (2018) 323-37.
[37] S.T. Smith, H. Zhang, Z. Wang. Influence of Frp Anchors on the Strength and Ductility of Frp-Strengthened Rc Slabs. Constr Build Mater 49 (2013) 998-1012.
[38] T.M. Pham, H. Hao. Behavior of Fiber-Reinforced Polymer-Strengthened Reinforced Concrete Beams under Static and Impact Loads. International Journal of Protective Structures 8 (1) (2017) 3-24.
[39] C. Czaderski, K. Soudki, M. Motavalli. Front and Side View Image Correlation Measurements on Frp to Concrete Pull-Off Bond Tests. J Compos Constr 14 (4) (2010) 451-63.
[40] M.S. Salimian, D. Mostofinejad. Experimental Evaluation of Cfrp-Concrete Bond Behavior under High Loading Rates Using Particle Image Velocimetry Method. J Compos Constr 23 (3) (2019) 04019010.
[41] C. Yuan, W. Chen, T.M. Pham, H. Hao. Effect of Aggregate Size on Bond Behaviour between Basalt Fibre Reinforced Polymer Sheets and Concrete. Compos B Eng 158 (2019c) 459-74.
[42] C. Pellegrino, D. Tinazzi, C. Modena. Experimental Study on Bond Behavior between Concrete and Frp Reinforcement. J Compos Constr 12 (2) (2008) 180-9.
[43] Y.-F. Wu, C. Jiang. Quantification of Bond-Slip Relationship for Externally Bonded Frp-to-Concrete Joints. J Compos Constr 17 (5) (2013) 673-86.

[44] J.G. Dai, T. Ueda, Y. Sato. Development of the Nonlinear Bond Stress–Slip Model of Fiber Reinforced Plastics Sheet–Concrete Interfaces with a Simple Method. J Compos Constr 9 (1) (2005) 52-62.
[45] Y.-F. Wu, X.-S. Xu, J.-B. Sun, C. Jiang. Analytical Solution for the Bond Strength of Externally Bonded Reinforcement. Compos Struct 94 (11) (2012) 3232-9.
[46] Y.-W. Zhou, Y.-F. Wu, Y. Yun. Analytical Modeling of the Bond–Slip Relationship at Frp-Concrete Interfaces for Adhesively-Bonded Joints. Compos B Eng 41 (6) (2010) 423-33.
[47] J. Vaculik, A.B. Sturm, P. Visintin, M.C. Griffith. Modelling Frp-to-Substrate Joints Using the Bilinear Bond-Slip Rule with Allowance for Friction—Full-Range Analytical Solutions for Long and Short Bonded Lengths. Int J Solids Struct 135 (2018) 245-60.
[48] J. Chen, J. Teng. Shear Capacity of Frp-Strengthened Rc Beams: Frp Debonding. Constr Build Mater 17 (1) (2003) 27-41.
[49] Y.-F. Wu, L. He. Width Effect of Interfacial Bond Characteristics. Constr Build Mater 220 (2019) 712-26.